Manifestation of vibronic dynamics in infrared spectra of Mott insulating fullerides

Yuki Matsuda, Naoya Iwahara, Katsumi Tanigaki, and Liviu F. Chibotaru

Manifestation of vibronic dynamics in infrared spectra of Mott insulating fullerides

Yuki Matsuda,[1, 2] Naoya Iwahara,[1, *] Katsumi Tanigaki,[2, 3] and Liviu F. Chibotaru[1, †]

[1] *Theory of Nanomaterials Group, University of Leuven, Celestijnenlaan 200F, B-3001 Leuven, Belgium*
[2] *Department of Physics, Graduate School of Science, Tohoku University,*
6-3 Aramaki, aza-Aoba, Aoba-ku, Sendai 980-8578, Japan
[3] *WPI-Advanced Institute for Materials Research (WPI-AIMR),*
Tohoku University, 2-1-1 Katahira, Aoba-ku, Sendai, 980-8577, Japan
(Dated: September 19, 2018)

The fine structure and temperature evolution of infrared spectra have been intensively used to probe the nature of Jahn-Teller dynamics in correlated materials. At the same time, theoretical framework to adequately extract the information on the complicated vibronic dynamics from infrared spectra is still lacking. In this work, the first-principles theory of the infrared spectra of dynamical Jahn-Teller system is developed and applied to the Mott-insulating Cs_3C_{60}. With the calculated coupling parameters for Jahn-Teller and infrared active vibrational modes, the manifestation of the dynamical Jahn-Teller effect in infrared spectra is elucidated. In particular, the temperature evolution of the infrared line shape is explained. The transformation of the latter into Fano resonance type in metallic fulleride is discussed on the basis of obtained results.

I. INTRODUCTION

The role of dynamical Jahn-Teller (JT) effect [1–3] in electronic property of correlated materials attracts significant attention. Such materials of current interest include e.g. various transition metal compounds [4–8], rare-earth [9] and actinide dioxides [10]. An increasing precision of the investigation of such materials demands detailed knowledge of the nature of JT dynamics and the mechanisms of its manifestation in observed properties. Rich fine structures in infrared (IR) spectra are expected to encode the information on the local JT dynamics. Despite the fact that IR spectroscopy has been applied to various systems [11–20], the relation between the JT dynamics and the structure of IR spectra has not been established. One family of materials where the JT effect has been much investigated are the alkali-doped fullerides [15, 16, 18, 21–29].

Recently, the understanding of the dynamical JT effect on the C_{60}^{3-} sites of alkali-doped fullerides A_3C_{60} (A = K, Rb, Cs) has significantly advanced. The accurate calculation of the orbital vibronic coupling parameters for C_{60} anions [30] enables to access realistic low-energy vibronic spectra of C_{60}^{n-} (n = 1-5) [31, 32]. Since dynamical JT (vibronic) state is expressed by a quantum superposition of statically JT deformed molecular wave functions over the directions in configuration space [1–3, 23, 25, 29], it is simultaneously characterized by the presence of the JT split adiabatic orbitals and the equal contributions of the degenerate electronic states to it. Therefore, the presence of the unquenched JT dynamics in Mott-insulating phase due to a large dynamical JT stabilization energy naturally explains the absence of orbital ordering and the isotropic character of the antiferromagnetic exchange interaction [26, 31]. The dynamical JT effect was found

not to be quenched by band effects in the metallic phase [33], a fact confirmed indirectly by experiment [18]. Since each C_{60}^{3-} site has nondegenerate three adiabatic orbitals, the conduction band of A_3C_{60} is also split into three inequivalent subbands. As a consequence, the electron correlation basically develops only in one JT split half-filled adiabatic subband (see Fig. 2d in Ref. [34]), and hence the critical intrafullerene electron repulsion for the JT-induced orbital-selective Mott transition is small [33] [35], which is consistent with the recent estimate of Coulomb repulsion by electrical conductivity measurements [36]. Based on the derived vibronic structure of fullerene anions, it was also shown that the spin-gap from NMR data [37, 38] is well reproducible [32].

The IR measurements of A_3C_{60} have been performed across the Mott transition. In the Mott insulating phase, the temperature dependence of the IR spectra was attributed to the evolution of the JT dynamics due to the variation of the structure of the adiabatic potential energy surface by thermal expansion of the crystal [15, 16]. The spectral shape in metallic phase close to the Mott transition remains similar to that in Mott insulating phase, whereas it gradually changes to Fano resonance type as departing from it [18]. The unchanged shape of the IR spectrum in the vicinity of Mott transition was interpreted as the evidence of the JT effect on C_{60}^{3-}, following the theoretical prediction [33]. On the other hand, the evolution of the Lorenzian shape into Fano resonance deep in metallic phase was interpreted in Ref. [18] as a quenching of JT effect, which contradicts the theoretical calculations [33] [39] and NMR [37, 40] and electrical conductivity [36] measurements: The NMR measurements show the spin gap induced by the JT dynamics in metallic Rb_3C_{60} [37] and the same magnetic properties in both Mott insulating phase and high temperature paramagnetic insulating phase above metallic one [40] and the electrical conductivity measurements show no drastic change of resistivity in the whole metallic domain [36]. In order to correctly assess the na-

ture of JT dynamics from the fine structure of IR spectra, it is decisive to develop a theoretical framework for their adequate treatment.

In this work, a fully quantum mechanical theory for IR spectra of dynamical JT systems is developed. Combining the developed theory and first-principles calculations, the IR active vibronic states of Cs_3C_{60} cluster are derived and, on this basis, IR spectra are simulated. In terms of the obtained vibronic states, the relation between the JT dynamics and the temperature evolution of IR spectra is revealed. The developed theoretical scheme will be indispensable for the understanding of the phenomena related to the photoexcitation processes in fullerides and other dynamical JT materials.

II. MODEL VIBRONIC HAMILTONIAN OF C_{60}^{3-}

The minimal model describing the manifestation of the JT dynamics in IR spectra is derived. Below, the irreducible representations (irrep) of I_h group are used, the components of the irreps. are always real in the main text, and the lower (upper) case is used for the irrep of the one electron orbital state and the mass-weighted normal mode (electronic term and vibronic states). Three orthogonal C_2 axes are chosen as the Cartesian axes (see Fig. S1 [41]).

In the low-energy states of C_{60}^{3-} site in A_3C_{60}, triply degenerate t_{1u} lowest unoccupied molecular orbitals (LUMO) are half-filled because of the deep LUMO levels and large separation from the other levels. The bielectronic interaction between electrons occupying the LUMOs, $\hat{H}_{bi}$, induces the term splitting as $^4A_u \oplus {}^2T_{1u} \oplus {}^2H_u$. $\hat{H}_{bi}$ raises the $^2T_{1u}$ term by $2J_H$ with respect to the ^2H_u term, where J_H is the Hund's rule coupling parameter (≈ 40 meV [31, 32, 42]). The t_{1u} orbitals couple to the totally symmetric a_g and the five-fold degenerate h_g vibrations of the C_{60} cage, and the linear vibronic coupling to the h_g modes, $\hat{H}_{vibro}^{(1)}$, gives rise to the JT effect [1, 3, 23, 25].

Within the simplest model for C_{60}^{3-} consisting of $\hat{H}_{bi}$, the Hamiltonian of harmonic oscillations, $\hat{H}_0$, and $\hat{H}_{vibro}^{(1)}$,

$$\hat{H}^{(0)} = \hat{H}_{bi} + \hat{H}_0 + \hat{H}_{vibro}^{(1)}, \tag{1}$$

the IR active t_{1u} vibrational degrees of freedom are uncoupled from the JT dynamics. Therefore, neither fine structure nor temperature evolution in IR spectra can be expected. In order to reveal the role of the JT dynamics in the IR spectra, the interplay of the vibronic and the IR vibrational degrees of freedom has to be considered. The interplay arises from nonlinear vibronic couplings admixing the IR modes. Although the t_{1u} LUMOs do not linearly couple to the IR active t_{1u} modes, they do to the products of the coordinates when the latter include the h_g representation (see Table S2 [41]). Thus, the minimal model should contain the quadratic vibronic term to the IR active modes allowing to indirectly relate the

TABLE I. Calculated quadratic vibronic coupling parameters $V_{\nu\mu_1\mu_2}^{\Gamma_1\Gamma_2}$ ($\times 10^{-7}$ a.u.).

$\Gamma_1(\mu_1)$	$\Gamma_2(\mu_2)$	$V_{\mu_1\mu_2}^{\Gamma_1\Gamma_2}$	$\Gamma_1(\mu_1)$	$\Gamma_2(\mu_2)$	ν	$V_{\nu\mu_1\mu_2}^{\Gamma_1\Gamma_2}$
$t_{1u}(4)$	$t_{1u}(4)$	-3.57	$g_u(5)$	$h_u(6)$	1	1.19
	$g_u(5)$	3.19			2	1.60
	$g_u(6)$	0.38	$g_u(6)$	$g_u(6)$	-	1.46
	$h_u(6)$	6.18	$h_u(6)$	$h_u(6)$	1	2.16
$g_u(5)$	$g_u(5)$	-1.89			2	3.23

IR and JT modes via electronic orbitals,

$$\hat{H} = \hat{H}^{(0)} + \hat{H}_{vibro}^{(2)}, \tag{2}$$

where,

$$\hat{H}_{vibro}^{(2)} = \sum_{\mu_i\Gamma_i} \sum_{\nu\gamma} \sum_{\lambda\lambda'} V_{\nu\mu_1\mu_2}^{\Gamma_1\Gamma_2} \{\hat{q}_{\Gamma_1(\mu_1)} \otimes \hat{q}_{\Gamma_2(\mu_2)}\}_{\nu h_g\gamma}$$

$$\times \sqrt{\frac{15}{2}} \langle t_{1u}\lambda | h_u\lambda', h_g\gamma \rangle |T_{1u}\lambda\rangle\langle H_u\lambda'| + h.c. \tag{3}$$

Here, $|T_{1u}\lambda\rangle$ ($\lambda = x, y, z$) and $|H_u\lambda'\rangle$ ($\lambda' = \theta, \epsilon, \xi, \eta, \zeta$ which stand for $(2z^2 - x^2 - y^2)/\sqrt{6}$, $(x^2 - y^2)/\sqrt{2}$, $\sqrt{2}yz$, $\sqrt{2}zx$, $\sqrt{2}xy$, respectively) are electronic term states, $\hat{q}_{\Gamma\gamma}$ is nuclear mass-weighted normal coordinate operator [43], $V_{\nu\mu_1\mu_2}^{\Gamma_1\Gamma_2}$ is the quadratic orbital vibronic coupling parameter, $\{\hat{q}_{\Gamma_1(\mu_1)} \otimes \hat{q}_{\Gamma_2(\mu_2)}\}_{\nu h_g\gamma}$ is the symmetrized product of corresponding nuclear coordinates [see Eq. (A1) and Ref.[1]], ν distinguishes multiple h_g representations since I_h is not simply reducible group, and $\langle t_{1u}\lambda | h_u\lambda', h_g\gamma \rangle$ is the Clebsch-Gordan coefficient (Sec. I in Ref. [41]). The coefficient $\sqrt{15/2}$ in Eq. (3) is introduced as in Refs. [3, 23, 25]. The absence of the diagonal block in $\hat{H}_{vibro}^{(2)}$ is due to the seniority selection rule [44]. In $\hat{H}_{vibro}^{(2)}$, the quadratic JT coupling is not included because it does not influence much the vibronic states of C_{60}^{3-} [45]. See for the derivation of Eq. (3) Appendix A 1.

III. NONLINEAR VIBRONIC COUPLING CONSTANTS

The frequencies $\omega_{\Gamma(\mu)}$ and orbital vibronic coupling parameters $V_{\nu\mu_1\mu_2}^{\Gamma_1\Gamma_2}$ of Cs_3C_{60} clusters were calculated using density functional theory (DFT) with hybrid exchange-correlation functional (Appendix B 1). Since the IR peak of the highest frequency mode ($\omega_{t_{1u}(4)} \approx 1360$ cm^{-1}) has the richest fine structure [15, 16, 18], we will describe only this peak. The obtained parameters for A15 and fcc lattices of Cs_3C_{60} are similar to each other, hence the parameters for A15 are used below. The calculated frequencies for neutral C_{60} are in line with experimental data (Table S3 [41]). Upon doping, the frequency of the $t_{1u}(4)$ mode shows relatively large red shift by about 60 cm^{-1} and approaches to the frequencies of $g_u(5)$

and $h_u(6)$ modes, $\omega_{t_{1u}(4)} = 1384$, $\omega_{g_u(5)} = 1334$, and $\omega_{h_u(6)} = 1351$ cm^{-1}. On the other hand, the $g_u(6)$ mode whose frequency is close to that of $t_{1u}(4)$ in the neutral C$_{60}$, implying a relevance to the spectra [15], does not vary much, $\omega_{g_u(6)} = 1440$ cm^{-1}. This result points to the importance of $t_{1u}(4)$, $g_u(5)$, and $h_u(6)$ rather than $g_u(6)$ for the description of the IR spectrum because these IR and JT inactive modes (g_u, h_u) may couple nonlinearly to the t_{1u} orbitals (see for the polarization vectors Fig. S1 [41]).

The quadratic orbital vibronic coupling parameters $V_{\nu\mu_1\mu_2}^{\Gamma_1\Gamma_2}$ (a.u.) were derived by fitting the t_{1u} LUMO levels with respect to the $t_{1u}z, g_u z, h_u\theta$ deformations (a.u.) to the model vibronic Hamiltonian (see for the model Hamiltonian Appendix A 2, for the fitting Fig. S2 in Ref. [41], and for the coupling parameters Table I). One should note that the magnitudes of $V_{\nu\mu_1\mu_2}^{\Gamma_1\Gamma_2}$, not only for the IR active $t_{1u}(4)$ mode but also for the IR inactive $g_u(5)$ and $h_u(6)$ modes, are similar to each other [46]. Indeed, the largest parameter is obtained for the t_{1u} and h_u modes. On the other hand, the intermode coupling involving the $t_{1u}(4)$ and $g_u(6)$ is found to be weak. Given the relatively large difference in frequency between them, the contribution from the $g_u(6)$ mode to the vibronic states is negligible. Thus, hereafter, we consider only the $t_{1u}(4)$, $g_u(5)$ and $h_u(6)$ modes which we call IR modes for simplicity [47] as well as the JT active h_g modes.

IV. VIBRONIC STATES

Comparing the energy scales of the linear and quadratic vibronic coupling, the latter is regarded as perturbation to the former [39]. The eigenstates of the unperturbed Hamiltonian, Eq. (1), are the direct products of the linear JT state [48], $|\Phi_\kappa^{(0)}\rangle$, and of the harmonic oscillations of the IR modes [43], $|\boldsymbol{n}'\rangle$. The JT states κ are characterized by the irrep Γ (or vibronic angular momentum J), its component γ, parity P originating from the seniority, and principal quantum number α distinguishing the energy levels, $\kappa = (\alpha\Gamma\gamma P)$ [31, 32]. The ground ($\Gamma = T_{1u}$, $P = +1$) and the first excited (H_u, -1) JT states are separated by about 8 meV and the other JT levels appear at > 30 meV.

The JT dynamics modifies the strengths of the nonlinear vibronic terms,

$$\hat{H}_{\text{vibro}}^{(2)} = \sum_{\mu_i\Gamma_i}\sum_{\nu\gamma}\sum_{\kappa\kappa'} V_{\nu\mu_1\mu_2}^{\Gamma_1\Gamma_2} \Xi(\kappa;\kappa')\{\hat{q}_{\Gamma_1(\mu_1)} \otimes \hat{q}_{\Gamma_2(\mu_2)}\}_{\nu h_g\gamma}$$

$$\times \sqrt{\frac{15}{2}}\langle\Gamma_\kappa\gamma_\kappa|\Gamma_{\kappa'}\gamma_{\kappa'}, h_g\gamma\rangle|\Phi_\kappa^{(0)}\rangle\langle\Phi_{\kappa'}^{(0)}|, \quad (4)$$

where, the electronic basis in Eq. (3) is replaced by the JT states (see Appendix A 3). The form remains the same as Eq. (3) except for the factor $\Xi(\kappa;\kappa')$ which is a vibronic factor modifying the operators (see e.g., Refs. [1–3]). For the lowest two JT states, $\Xi = 0.63$ [32], and thus, the quadratic vibronic coupling is reduced (for
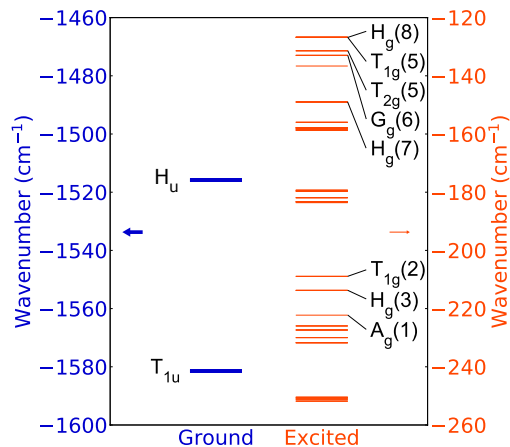

FIG. 1. Low-energy vibronic levels mainly originating from the lowest JT states. Left column shows the lowest JT levels without excitation of the IR modes. The right column shows the vibronic levels with one vibrational excitation of the IR modes.

other Ξ's, see Table S4 [41]). Besides the reduction factor, the parity selection rule reduces the effect of the quadratic coupling because the coupling is only operative between the linear JT states with different parities (see Sec. IV B 3 in Ref. [32]).

The eigenstates of the full Hamiltonian, Eq. (2), which we call vibronic states [46], are expressed as:

$$|\Psi_\tau\rangle = \sum_\kappa\sum_{\boldsymbol{n}'} C_{\kappa\boldsymbol{n}';\tau}|\Phi_\kappa^{(0)}\rangle \otimes |\boldsymbol{n}'\rangle, \quad (5)$$

where, $C_{\kappa\boldsymbol{n}';\tau}$ are coefficients. The vibronic state τ is also characterized by the principal quantum number, irrep and its component.

The vibronic states were numerically derived (Appendix B 2). The obtained low-energy vibronic levels are shown in Fig. 1 (see also Fig. S3 [41]). The lowest T_{1u} and H_u JT levels are not affected by $\hat{H}_{\text{vibro}}^{(2)}$, and thus, they are continued to be called JT states (left column in Fig. 1) The excited vibronic states arising from the T_{1u} and H_u JT states (right column in Fig. 1) are in a good approximation described by the symmetrized products of T_{1u}/H_u JT states and $|\boldsymbol{n}'\rangle$ involving only one IR vibrational excitation (see Appendix C and Table S5 [41]).

V. VIBRONIC EXCITATIONS IN INFRARED SPECTRA

The IR absorption corresponds to the transition from the JT to the excited vibronic states (left and right columns of Fig. 1, respectively). Introducing the coupling to the external electric field $\boldsymbol{E}$ [1, 2],

$$\hat{H}_{\text{IR}} = \sum_\mu \sum_{\gamma=x,y,z} Z_\mu \hat{q}_{t_{1u}(\mu)\gamma} E_\gamma, \quad (6)$$
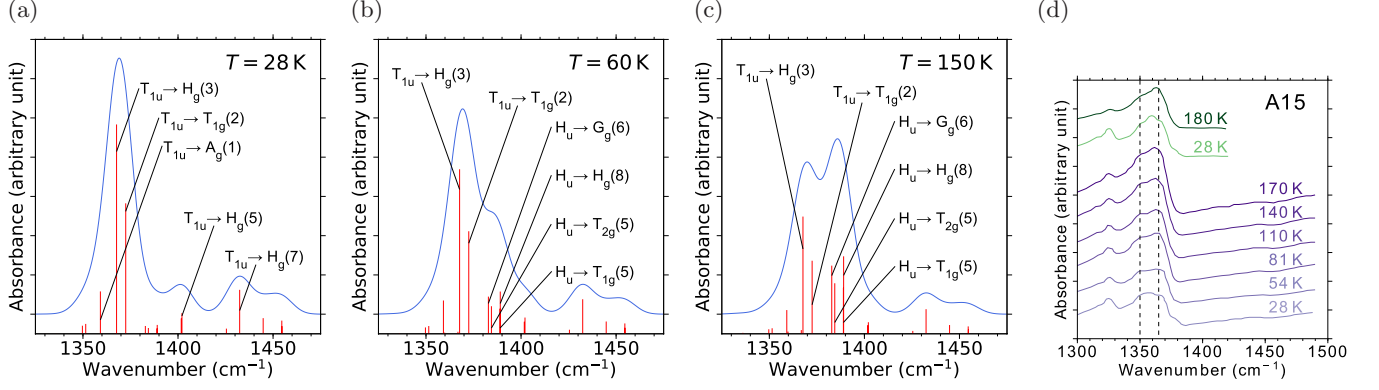
FIG. 2. (a)-(c) Theoretical and (d) experimental IR spectra of A15 Cs_3C_{60}. Calculated IR spectra of C_{60}^{3-} at (a) 28 K, (b) 60 K, and (c) 150 K. All intensities (red vertical lines) are integrated with a Gauss function of full width of half maxima = 14 cm^{-1} (blue). In (d), the upper two (green) and lower six (purple) spectra are taken from Ref. [15] and Ref.[16], respectively. The vertical dashed lines at 1350 and 1365 cm^{-1} show the positions of the peaks of our interest.

where Z_μ is effective nuclear charge, the IR absorbance is given by [49]:

$$I(\omega, T) \propto \sum_{\kappa\tau\gamma} \rho_\kappa(T)\omega \left|\langle\Psi_\tau|\hat{q}_{t_{1u}(4)\gamma}|\Psi_\kappa\rangle\right|^2 \delta\left(\omega - \omega_{\tau\kappa}\right), (7)$$

where, κ indicates the low-lying JT states, τ denotes the vibronic states with one IR excitation, $\rho_\kappa(T)$ is the canonical distribution at temperature T, and $\hbar\omega_{\tau\kappa} = E_\tau - E_\kappa$.

The simulated IR spectra of C_{60}^{3-} at (a) 28 K, (b) 60 K, and (c) 150 K are shown in Fig. 2. At 28 K, all the peaks are mainly composed of the excitations from the lowest T_{1u} JT level. The highest peak around 1370 cm^{-1} includes three major components corresponding to the excitations from the T_{1u} to $H_g(3)$, $T_{1g}(2)$, and $A_g(1)$ vibronic levels (Fig. 1 and Table S6 [41]). In these IR-admixed vibronic states, the products of the T_{1u} JT state and one $t_{1u}(4)$ vibrational excitation have large weight (Table S5 [41]). As temperature rises, the first excited H_u JT state is also thermally populated, and thus, the fraction of the transitions from the T_{1u} (H_u) JT state decreases (increases). The new peaks observed at high temperature correspond to the transitions from the H_u to the $G_g(6)$, $H_g(8)$, $T_{2g}(5)$ and $T_{1g}(5)$ vibronic levels (Fig. 1 and Table S6 [41]) which mainly originate from the products of the H_u JT state and one $t_{1u}(4)$ excitation (Table S5 [41]). The contributions from the H_u are not negligible already at 60 K and eventually become stronger at high temperature [Fig. 2 (b), (c)] [50]. The evolution explains the basic features of the experimental data: in the spectra, the peak around 1350 cm^{-1} from the T_{1u} JT level is the highest at $T = 28$ K, while the peak at 1365 cm^{-1} from the H_u JT level becomes higher as temperature increases [Fig. 2 (d)] [51]. Thus, the present theory proves that the temperature dependence indeed originates from thermal population of vibronic excitation from the T_{1u} to the H_u JT states. Besides the main peaks, some of the other fine structures can be explained. For example, the gradual decrease of the peak

at 1400 cm^{-1} [$T_{1u} \rightarrow H_g(5)$] with the increase of temperature resembles the temperature dependence of the shoulder at 1380 cm^{-1} in the experimental data [Fig. 2 (d)]. Note that such small structures arises due to the quadratic vibronic coupling involving IR inactive g_u/h_u modes besides IR active t_{1u}.

VI. DISCUSSION

The interpretation of the IR spectra of JT systems is often based on the modification of selection rules due to the symmetry lowering [52]. Thus, in the previous quantum chemistry study of Cs_3C_{60} cluster, the IR spectra were calculated for some electronic configurations at statically deformed structure [53]. Considering the complicated orbital-lattice entangled nature of vibronic states, such simplified treatment is not sufficient to reveal the mechanisms of the implication of dynamical JT effect in the observed properties. The theoretical framework for a complete treatment of the JT dynamics and IR spectra in high symmetric JT systems is established in this work. On this basis, it is shown that the assumption of a change of adiabatic potential energy surface by thermal expansion [15, 16] is not necessary for the description of the temperature evolution of IR spectra.

The obtained results can be applied to the analysis of the IR spectra in fullerides close to Mott transition where the IR spectra are practically unaffected by weak intersite interactions. In the metallic phase, the electron transfer interaction $\hat{H}_t$ is not negligible. In the ground state, $\hat{H}_t$ forms continuous vibronic states without quenching the JT dynamics because of the large stabilization energy of the latter [33]. As a consequence, the spin gap induced by the JT dynamics is observed even in the fullerides with small lattice constant [37]. The IR-admixed vibronic states (right column of Fig. 1) are also mixed with many excited vibronic states involving one IR vi-

brational excitation by $\hat{H}_t$. At a sufficiently strong interaction of the excited vibronic states with a continuum of bulk states, a Fano resonance in IR spectra will appear. We stress that the modification of the shape of IR spectra into a Fano resonance [18] does not necessarily mean the quench of JT effect in the ground state.

The present work can also contribute to the description of the light-induced superconductivity in K_3C_{60} [54, 55]. The model used in recent works [56, 57] for the discussion of possible mechanism based on a simplified quadratic vibronic coupling, should be replaced with Eq. (2). In Ref. [54], the importance of the cubic coupling was also proposed to relate the vibration of IR active t_{1u} mode and JT distortion, while it was shown here that these lattice degrees of freedom are already entangled (5) within the quadratic vibronic model via degenerate electronic terms.

VII. CONCLUSION

The quantum mechanical framework for the description of the IR spectra of dynamical JT system is developed. Based on the first-principles calculations, the nonlinear vibronic Hamiltonian of C_{60}^{3-} site was derived, and the vibronic states involving both the JT and IR degrees of freedom were calculated. On this basis, the relation between the temperature evolution of IR spectra in Mott insulating Cs_3C_{60} and JT dynamics was established. The first-principles calculations also showed non-negligible nonlinear vibronic couplings between the IR active t_{1u} mode and non-IR active g_u and h_u modes, giving rise to the fine structures of the IR spectra. It is worthy to note that, contrary to the previous approaches, static JT distortions are not assumed to be responsible for the temperature evolution of IR spectra as well as their fine structure. Because the fine structure of the IR spectra is governed by the IR-admixed vibronic structure, the reconsideration on the relation between the IR spectra in metallic fullerides and the nature of JT dynamics as function of their volume is required. The developed theoretical approach can be applied to the study of the spectroscopic and light-induced electronic properties of various correlated dynamical JT materials.

Appendix A: Quadratic vibronic coupling

In this section, SO(3) symmetry and the spherical basis for the t_{1u} and $h_{u/g}$ irreps. of I_h group are used. The Condon-Shortley's phase convention is taken for the spherical harmonics [58].

1. Derivation of Eq. (3)

The t_{1u} LUMOs couple to the symmetrized h_g polynomials of the normal coordinates. The quadratic h_g polynomials are calculated as

$$\{\hat{q}_{\Gamma_1(\mu_1)} \otimes \hat{q}_{\Gamma_2(\mu_2)}\}_{\nu h_g \gamma} = \sum_{\gamma_1 \gamma_2} \langle \nu h_g \gamma | \Gamma_1 \gamma_1 \Gamma_2 \gamma_2 \rangle \\ \times \hat{q}_{\Gamma_1(\mu_1)\gamma_1} \hat{q}_{\Gamma_2(\mu_2)\gamma_2}, \quad (A1)$$

where the sum is over the components of the irreps. Γ_1 and Γ_2. See for the explicit form Sec. II in Ref. [41]. The quadratic vibronic coupling is expressed as

$$\hat{H}_{vibro}^{(2)} = \sum_{\mu_i \Gamma_i} \sum_{\nu \gamma} \sum_{\lambda \lambda' \sigma} V_{\nu \mu_1 \mu_2}^{\Gamma_1 \Gamma_2} \{\hat{q}_{\Gamma_1(\mu_1)} \otimes \hat{q}_{\Gamma_2(\mu_2)}\}_{\nu h_g \gamma} \\ \times \sqrt{\frac{5}{2}} \langle t_{1u}\lambda | t_{1u}\lambda', h_g\gamma \rangle \hat{c}_{t_{1u}\lambda\sigma}^\dagger \hat{c}_{t_{1u}\lambda'\sigma}, \quad (A2)$$

where σ indicates the projection of electron spin and $\hat{c}_{t_{1u}\lambda\sigma}^\dagger$ and $\hat{c}_{t_{1u}\lambda\sigma}$ are the electron creation and annihilation operators in spin-orbital $t_{1u}\lambda\sigma$. Transforming the real components of the irreps. into the spherical ones, Eq. (A2) reduces to the same form as Eq. (A1) in Ref. [32]. Thus, by the same procedure as described in the Appendix A in Ref. [32], we obtain the spherical form of Eq. (3):

$$\hat{H}_{vibro}^{(2)} = \sum_{\mu_i \Gamma_i} \sum_{\nu m''} \sum_{nn'} (-1)^{m''} V_{\nu \mu_1 \mu_2}^{\Gamma_1 \Gamma_2} \\ \times \{\hat{q}_{\Gamma_1(\mu_1)} \otimes \hat{q}_{\Gamma_2(\mu_2)}\}_{\nu 2, -m''} \sqrt{\frac{15}{2}} \langle 1n | 2n', 2m'' \rangle \\ \times \left[|1n\rangle\langle 2n'| - (-1)^{m''} |2, -n'\rangle\langle 1, -n| \right], \quad (A3)$$

where, $|1n\rangle$ and $|2n'\rangle$ express the spherical form of the T_{1u} and H_u multiplet states, respectively, and n, n', m'' the projections of the angular momenta. By the inverse transformation from the spherical into the Cartesian basis, we obtain Eq. (3). The difference in the coefficients in Eqs. (3), (A3) and Eq. (A2) by $\sqrt{3}$ comes from the reduced matrix element of Racah's $\hat{U}^{(2)}$ operator. Since the spin and orbital degrees of freedom are independent from each other, Eqs. (3) and (A3) show only the orbital part.

2. Model Hamiltonian for the IR modes

One-electron quadratic vibronic Hamiltonian for the IR modes is given by

$$\hat{H}'_0 + \hat{H}^{(2)\prime}_{\mathrm{vibro}} = (|t_{1u}x\rangle, |t_{1u}y\rangle, |t_{1u}z\rangle)$$

$$\times \left(\mathbf{H}'_0 + \mathbf{H}^{(2)\prime}_{\mathrm{vibro}}\right) \begin{pmatrix} \langle t_{1u}x| \\ \langle t_{1u}y| \\ \langle t_{1u}z| \end{pmatrix}. \quad (A4)$$

$$\mathbf{H}'_0 = \left(\epsilon_{t_{1u}} + \sum_{\gamma=x,y,z} \frac{k_{t_{1u}(4)}}{2} q^2_{t_{1u}(4)\gamma} + \sum_{\gamma=a,x,y,z} \frac{k_{g_u(5)}}{2} q^2_{g_u(5)\gamma} + \sum_{\gamma=\theta,\xi,\eta,\zeta} \frac{k_{h_u(6)}}{2} q^2_{h_u(6)\gamma}\right)\mathbf{I}, \quad (A5)$$

$$\mathbf{H}^{(2)\prime}_{\mathrm{vibro}} = \sum_{\gamma=\theta,\epsilon,\xi,\eta,\zeta} \left(V^{t_{1u}t_{1u}}_{44}\{\hat{q}_{t_{1u}(4)} \otimes \hat{q}_{t_{1u}(4)}\}_{h_g\gamma} + V^{g_u g_u}_{55}\{\hat{q}_{g_u(5)} \otimes \hat{q}_{g_u(5)}\}_{h_g\gamma} + \sum_{\nu=1,2} V^{h_u h_u}_{\nu 66}\{\hat{q}_{h_u(6)} \otimes \hat{q}_{h_u(6)}\}_{\nu h_g\gamma}\right.$$

$$\left. + 2V^{t_{1u}g_u}_{45}\{\hat{q}_{t_{1u}(4)} \otimes \hat{q}_{g_u(5)}\}_{h_g\gamma} + 2V^{t_{1u}h_u}_{46}\{\hat{q}_{t_{1u}(4)} \otimes \hat{q}_{h_u(6)}\}_{h_g\gamma} + \sum_{\nu=1,2} 2V^{g_u h_u}_{\nu 56}\{\hat{q}_{g_u(5)} \otimes \hat{q}_{h_u(6)}\}_{\nu h_g\gamma}\right)\mathbf{M}_\gamma, (A6)$$

$k_{\Gamma(\mu)}$ indicates the elastic parameter, $\mathbf{I}$ is the three-dimensional unit matrix, and

$$\mathbf{M}_\theta = \begin{pmatrix} \frac{1}{2} & 0 & 0 \\ 0 & \frac{1}{2} & 0 \\ 0 & 0 & -1 \end{pmatrix}, \quad \mathbf{M}_\epsilon = \begin{pmatrix} -\frac{\sqrt{3}}{2} & 0 & 0 \\ 0 & \frac{\sqrt{3}}{2} & 0 \\ 0 & 0 & 0 \end{pmatrix},$$

$$\mathbf{M}_\xi = \begin{pmatrix} 0 & 0 & 0 \\ 0 & 0 & -\frac{\sqrt{3}}{2} \\ 0 & -\frac{\sqrt{3}}{2} & 0 \end{pmatrix}, \quad \mathbf{M}_\eta = \begin{pmatrix} 0 & 0 & -\frac{\sqrt{3}}{2} \\ 0 & 0 & 0 \\ -\frac{\sqrt{3}}{2} & 0 & 0 \end{pmatrix},$$

$$\mathbf{M}_\zeta = \begin{pmatrix} 0 & -\frac{\sqrt{3}}{2} & 0 \\ -\frac{\sqrt{3}}{2} & 0 & 0 \\ 0 & 0 & 0 \end{pmatrix}. \quad (A7)$$

In Eqs. (A5) and (A6), only the IR modes [43] are included.

3. Derivation of Eq. (4)

The transformation from Eq. (3) to Eq. (4) is described here. In this subsection, to make use of the SO(3) symmetry of the linear $t^3_{1u} \otimes h_g$ JT system, the vibronic angular momentum J is used instead of real irrep Γ of I_h group.

Using the identity operator for the JT states, $\hat{I}^{(0)} = \sum_{\alpha JmP} |\Phi^{(0)}_{\alpha JmP}\rangle\langle\Phi^{(0)}_{\alpha JmP}|$,

$$\hat{H}^{(2)}_{\mathrm{vibro}} = \hat{I}^{(0)} \hat{H}^{(2)}_{\mathrm{vibro}} \hat{I}^{(0)}$$

$$= \sum_{\alpha JmP} \sum_{\alpha' J'm'P'} \langle\Psi^{(0)}_{\alpha JmP}|\hat{H}^{(2)}_{\mathrm{vibro}}|\Psi^{(0)}_{\alpha' J'm'P'}\rangle$$

$$\times |\Psi^{(0)}_{\alpha JmP}\rangle\langle\Psi^{(0)}_{\alpha' J'm'P'}|, \quad (A8)$$

Here, the projection of the electron spin is omitted, $\mathbf{H}'_0$ involves the orbital energy $\epsilon_{t_{1u}}$ and the harmonic oscillator terms, and $\mathbf{H}^{(2)\prime}_{\mathrm{vibro}}$ is the quadratic vibronic coupling:

where, J is the vibronic angular momentum and m is its projection. Substituting Eq. (A3) into the matrix element of Eq. (A8), we obtain

$$\hat{H}^{(2)}_{\mathrm{vibro}} = \sum_{\alpha JmP} \sum_{\alpha' J'm'P'} \sum_{\mu_i\Gamma_i} \sum_{\nu m''} V^{\Gamma_1\Gamma_2}_{\nu\mu_1\mu_2}$$

$$\times (-1)^{m''}\{\hat{q}_{\Gamma_1(\mu_1)} \otimes \hat{q}_{\Gamma_2(\mu_2)}\}_{\nu 2,-m''}\sqrt{\frac{15}{2}}$$

$$\times \langle\Psi^{(0)}_{\alpha JmP}|\hat{M}_{2m''}|\Psi^{(0)}_{\alpha' J'm'P'}\rangle|\Psi^{(0)}_{\alpha JmP}\rangle\langle\Psi^{(0)}_{\alpha' J'm'P'}|, \quad (A9)$$

with rank 2 irreducible tensor operator

$$\hat{M}_{2m''} = \sum_{nn'} \langle 1n|2n', 2m''\rangle$$

$$\times \left[|1n\rangle\langle 2n'| - (-1)^{m''}|2, -n'\rangle\langle 1, -n|\right]. (A10)$$

Applying Wigner-Eckart theorem [58] to the matrix elements of $\hat{M}_{2m''}$,

$$\langle\Psi^{(0)}_{\alpha Jm+}|\hat{M}_{2m''}|\Psi^{(0)}_{\alpha' J'm'-}\rangle$$

$$= \frac{\langle\Psi^{(0)}_{\alpha J+}\|\hat{M}_2\|\Psi^{(0)}_{\alpha' J'-}\rangle}{\sqrt{2J+1}}\langle Jm|J'm', 2m''\rangle$$

$$= \Xi(\alpha J+; \alpha' J'-)\langle Jm|J'm', 2m''\rangle. \quad (A11)$$

Here, the parities of the T_{1u} and H_u terms are defined to be $+1$ and -1, respectively [see Eq. (11) in Ref. [32]], and $\Xi(\alpha JP; \alpha' J'P')$ is defined by

$$\Xi(\alpha JP; \alpha' J'P') = \frac{\langle\Psi^{(0)}_{\alpha JP}\|\hat{M}_2\|\Psi^{(0)}_{\alpha' J'P'}\rangle}{\sqrt{2J+1}}. \quad (A12)$$

Therefore, by the substitution of Eq. (A11) into Eq. (A9), we obtain

$$
\begin{aligned}
\hat{H}_{\text{vibro}}^{(2)} &= \sum_{\alpha Jm} \sum_{\alpha' J'm'} \sum_{\mu_i \Gamma_i} \sum_{\nu m''} V_{\nu\mu_1\mu_2}^{\Gamma_1\Gamma_2} \Xi(\alpha J+; \alpha' J'-) \\
&\quad \times (-1)^{m''} \{\hat{q}_{\Gamma_1(\mu_1)} \otimes \hat{q}_{\Gamma_2(\mu_2)}\}_{\nu 2, -m''} \sqrt{\frac{15}{2}} \\
&\quad \times \langle Jm|J'm', 2m''\rangle |\Psi_{\alpha Jm+}^{(0)}\rangle\langle\Psi_{\alpha' J'm'-}^{(0)}| + \text{h.c.} \\
&= \sum_{\alpha JmP} \sum_{\alpha' J'm'P'} \sum_{\mu_i \Gamma_i} \sum_{\nu m''} V_{\nu\mu_1\mu_2}^{\Gamma_1\Gamma_2} \Xi(\alpha JP; \alpha' J'P') \\
&\quad \times (-1)^{m''} \{\hat{q}_{\Gamma_1(\mu_1)} \otimes \hat{q}_{\Gamma_2(\mu_2)}\}_{\nu 2, -m''} \sqrt{\frac{15}{2}} \\
&\quad \times \langle Jm|J'm', 2m''\rangle |\Psi_{\alpha JmP}^{(0)}\rangle\langle\Psi_{\alpha' J'm'P'}^{(0)}|. \quad \text{(A13)}
\end{aligned}
$$

To obtain the second form,

$$
\begin{aligned}
\left[\{\hat{q}_{\Gamma_1(\mu_1)} \otimes \hat{q}_{\Gamma_2(\mu_2)}\}_{\nu 2, -m''}\right]^\dagger \\
= (-1)^{m''} \{\hat{q}_{\Gamma_1(\mu_1)} \otimes \hat{q}_{\Gamma_2(\mu_2)}\}_{\nu 2 m''}, \quad \text{(A14)}
\end{aligned}
$$

and

$$
\begin{aligned}
\Xi(\alpha J+; \alpha' J'-)\langle Jm|J'm', 2m''\rangle \\
= \Xi(\alpha' J'-; \alpha J+)(-1)^{m''}\langle J'm'|Jm, 2, -m''\rangle \text{(A15)}
\end{aligned}
$$

are used. Nonzero $\Xi(\alpha J+; \alpha' J'-)$'s for the low-energy JT levels are shown in Table S4 [41]. Finally, using the relation between the irreps. of SO(3) and I_h in Eq. (A13), we obtain Eq. (4). For details of the relation of these two representations, see Sec. I A in the Supplemental Materials of Ref. [45].

Appendix B: Computational methods

1. DFT calculations

In order to determine the frequencies and the quadratic vibronic coupling parameters, DFT calculations of Cs_3C_{60} cluster were performed. The cluster consists of one C_{60}, the nearest Cs atoms and several tens of point charges for distant C_{60}^{3-} (-3) and Cs^+ ($+1$). For the calculations, B3LYP hybrid exchange-correlation functional was used with a triple-zeta polarization 6-311G(d) and double zeta 3-21G basis sets for C and Cs, respectively [59]. In order to avoid the artificial splitting of the t_{1u} orbital levels, the ^4A_u electronic configuration was treated within spin-unrestricted approach. The quadratic vibronic coupling constants were derived by fitting the t_{1u} LUMO levels with respect to the deformed structures to the model Hamiltonian, Eq. (A4). The results of the fitting are shown in Fig. S2 [41].

2. Calculation of vibronic states

The vibronic Hamiltonian matrix was derived using the JT states of Ref. [32], and then numerically diagonalized

[60]. The basis of $|\Psi_\tau\rangle$ (5) was truncated on the basis of the excitation energy of JT states and the number of vibrational excitations for IR modes [43]: the former was < 90 meV and the latter was 3,

$$
0 \leq \sum_{\Gamma(\mu)\gamma} n'_{\Gamma(\mu)\gamma} \leq 3, \quad \text{(B1)}
$$

where, the sum is over the IR modes, and $n'_{\Gamma(\mu)\gamma} \geq 0$ is vibrational quantum number. The cutoff of the JT states restricts the maximum temperature for the simulation of the IR spectra as in the case of spin gap [32] because the JT levels higher than the cutoff cannot be populated. The maximum temperature treated in this work is 150 K.

Appendix C: Assignment of the vibronic states

The lowest vibronic states (left column of Fig. 1) are expressed by the linear combinations of the products of the JT states and the vibrational vacuum $|\boldsymbol{n}' = \boldsymbol{0}\rangle$ or two vibrationally excited states of the IR modes [43]. The contribution from the latter is negligible in the present case, and thus, these low-energy vibronic states are well defined by the JT states.

On the other hand, the excited vibronic states (right column of Fig. 1) are described by the linear combination of the products of the JT states and the one- or three-vibrationally excited IR states, and the main contributions come from the former. Therefore, the excited vibronic states $|\Psi_\tau\rangle$ are assigned by the symmetrized products of the JT and the one vibrationally excited states. The symmetrized states are expressed as

$$
|(\Gamma_1\Gamma_2)n\Gamma\gamma\rangle = \sum_{\gamma_1\gamma_2} |\Gamma_1\gamma_1\rangle \otimes |\Gamma_2\gamma_2\rangle\langle\Gamma_1\gamma_1, \Gamma_2\gamma_2|\nu\Gamma\gamma\rangle,
$$

$$(C1)$$

where, Γ_1 and Γ_2 indicate the irreps. of the JT and IR states, respectively. Thus, Γ_2 is the irrep of the excited IR mode. The product states of the T_{1u} JT state and the t_{1u}, g_u, h_u vibrational states split into 10 states,

$$
\begin{aligned}
T_{1u} \otimes t_{1u} &= A_g \oplus T_{1g} \oplus H_g, \\
T_{1u} \otimes g_u &= T_{2g} \oplus G_g \oplus H_g, \\
T_{1u} \otimes h_u &= T_{1g} \oplus T_{2g} \oplus G_g \oplus H_g, \quad \text{(C2)}
\end{aligned}
$$

and those with the H_u JT state into 16 states,

$$
\begin{aligned}
H_u \otimes t_{1u} &= T_{1g} \oplus T_{2g} \oplus G_g \oplus H_g, \\
H_u \otimes g_u &= T_{1g} \oplus T_{2g} \oplus G_g \oplus 2H_g, \\
H_u \otimes h_u &= A_g \oplus T_{1g} \oplus T_{2g} \oplus 2G_g \oplus 2H_g, \quad \text{(C3)}
\end{aligned}
$$

respectively. The explicit forms of the symmetrized vibronic states (C1) are given in Sec. IV A of Ref. [41]. The contribution of each symmetrized state (C1) to the vibronic states $|\Psi_\tau\rangle$, Eq. (5), is quantitatively evaluated by calculating

$$
w(\Gamma_1\Gamma_2\nu\Gamma, \tau) = \langle\Psi_\tau|\hat{I}_{(\Gamma_1\Gamma_2)\nu\Gamma}|\Psi_\tau\rangle, \quad \text{(C4)}
$$

where, $\hat{I}_{(\Gamma_1\Gamma_2)\nu\Gamma}$ is the projector into the symmetrized states $(\Gamma_1\Gamma_2)\nu\Gamma\gamma$,

$$\hat{I}_{(\Gamma_1\Gamma_2)\nu\Gamma} = \sum_\gamma |(\Gamma_1\Gamma_2)\nu\Gamma\gamma\rangle\langle(\Gamma_1\Gamma_2)\nu\Gamma\gamma|. \quad \text{(C5)}$$

Eq. (C4) also enables us to skip the analysis of the structure of $|\Psi_\tau\rangle$ for the assignment. The list of $w(\Gamma_1\Gamma_2\nu\Gamma, \tau)$ are given in Table S5 [41].

[1] I. B. Bersuker and V. Z. Polinger, *Vibronic Interactions in Molecules and Crystals* (Springer–Verlag, Berlin, 1989).

[2] M. D. Kaplan and B. G. Vekhter, *Cooperative Phenomena in Jahn-Teller Crystals* (Plenum Press, New York and London, 1995).

[3] C. C. Chancey and M. C. M. O'Brien, *The Jahn–Teller Effect in C_{60} and Other Icosahedral Complexes* (Princeton University Press, Princeton, 1997).

[4] A. Krimmel, M. Mücksch, V. Tsurkan, M. M. Koza, H. Mutka, and A. Loidl, "Vibronic and Magnetic Excitations in the Spin-Orbital Liquid State of $FeSc_2S_4$," Phys. Rev. Lett. **94**, 237402 (2005).

[5] M. A. de Vries, A. C. Mclaughlin, and J.-W. G. Bos, "Valence Bond Glass on an fcc Lattice in the Double Perovskite Ba_2YMoO_6," Phys. Rev. Lett. **104**, 177202 (2010).

[6] S. Nakatsuji, K. Kuga, K. Kimura, R. Satake, N. Katayama, E. Nishibori, H. Sawa, R. Ishii, M. Hagiwara, F. Bridges, T. U. Ito, W. Higemoto, Y. Karaki, M. Halim, A. A. Nugroho, J. A. Rodriguez-Rivera, M. A. Green, and C. Broholm, "Spin-orbital short-range order on a honeycomb-based lattice," Science **336**, 559 (2012).

[7] K. Kamazawa, M. Ishikado, S. Ohira-Kawamura, Y. Kawakita, K. Kakurai, K. Nakajima, and M. Sato, "Interaction of spin-orbital-lattice degrees of freedom: Vibronic state of the corner-sharing-tetrahedral frustrated spin system $HoBaFe_4O_7$ by dynamical Jahn-Teller effect," Phys. Rev. B **95**, 104413 (2017).

[8] R. Nirmala, K.-H. Jang, H. Sim, H. Cho, J. Lee, N.-G. Yang, S. Lee, R. M. Ibberson, K. Kakurai, M. Matsuda, S.-W. Cheong, V. V. Gapontsev, S. V. Streltsov, and J.-G. Park, "Spin glass behavior in frustrated quantum spin system $CuAl_2O_4$ with a possible orbital liquid state," J. Phys. Condens. Matter **29**, 13LT01 (2017).

[9] C. H. Webster, L. M. Helme, A. T. Boothroyd, D. F. McMorrow, S. B. Wilkins, C. Detlefs, B. Detlefs, R. I. Bewley, and M. J. McKelvy, "Influence of static Jahn-Teller distortion on the magnetic excitation spectrum of PrO_2: A synchrotron x-ray and neutron inelastic scattering study," Phys. Rev. B **76**, 134419 (2007).

[10] P. Santini, S. Carretta, G. Amoretti, R. Caciuffo, N. Magnani, and G. H. Lander, "Multipolar interactions in f-electron systems: The paradigm of actinide dioxides," Rev. Mod. Phys. **81**, 807 (2009).

[11] S. Yamaguchi, Y. Okimoto, and Y. Tokura, "Local lattice distortion during the spin-state transition in $LaCoO_3$," Phys. Rev. B **55**, R8666 (1997).

[12] G. Klupp, K. Kamarás, N. M. Nemes, C. M. Brown, and J. Leão, "Static and dynamic Jahn-Teller effect in the alkali metal fulleride salts A_4C_{60} $(A = K, Rb, Cs)$," Phys. Rev. B **73**, 085415 (2006).

[13] S.-H. Jung, J.-H. Noh, J. Kim, C. L. Zhang, S. W. Cheong, and E. J. Choi, "Infrared phonon study of the $S = 1$ spinel oxide ZnV_2O_4," J. Phys. Condens. Matter **20**, 175205 (2008).

[14] E. A. Francis, S. Scharinger, K. Németh, K. Kamarás, and C. A. Kuntscher, "Pressure-induced transition from the dynamic to static Jahn-Teller effect in $(Ph_4P)_2IC_{60}$," Phys. Rev. B **85**, 195428 (2012).

[15] G. Klupp, P. Matus, K. Kamarás, A. Y. Ganin, A. McLennan, M. J. Rosseinsky, Y. Takabayashi, M. T. McDonald, and K. Prassides, "Dynamic Jahn-Teller effect in the parent insulating state of the molecular superconductor Cs_3C_{60}," Nat. Commun. **3**, 912 (2012).

[16] K. Kamarás, G. Klupp, P. Matus, A. Y. Ganin, A. McLennan, M. J. Rosseinsky, Y. Takabayashi, M. T. McDonald, and K. Prassides, "Mott localization in the correlated superconductor Cs_3C_{60} resulting from the molecular Jahn-Teller effect," J. Phys.: Conf. Ser. **428**, 012002 (2013).

[17] Z. Qu, Y. Zou, S. Zhang, L. Ling, L. Zhang, and Y. Zhang, "Spin-phonon coupling probed by infrared transmission spectroscopy in the double perovskite Ba_2YMoO_6," J. Appl. Phys. **113**, 17E137 (2013).

[18] R. H. Zadik, Y. Takabayashi, G. Klupp, R. H. Colman, A. Y. Ganin, A. Potočnik, P. Jeglič, D. Arčon, P. Matus, K. Kamarás, Y. Kasahara, Y. Iwasa, A. N. Fitch, Y. Ohishi, G. Garbarino, K. Kato, M. J. Rosseinsky, and K. Prassides, "Optimized unconventional superconductivity in a molecular Jahn-Teller metal," Sci. Adv. **1**, e1500059 (2015).

[19] E. Constable, R. Ballou, J. Robert, C. Decorse, J.-B. Brubach, P. Roy, E. Lhotel, L. Del-Rey, V. Simonet, S. Petit, and S. deBrion, "Double vibronic process in the quantum spin ice candidate $Tb_2Ti_2O_7$ revealed by terahertz spectroscopy," Phys. Rev. B **95**, 020415 (2017).

[20] V. Lavrentiev, D. Chvostova, I. Lavrentieva, J. Vacik, Y. Daskal, M. Barchuk, D. Rafaja, and A. Dejneka, "Optical transitions and electronic interactions in self-assembled cobalt-fullerene mixture films," J. Phys. D: Appl. Phys. **50**, 485305 (2017).

[21] O. Gunnarsson, "Superconductivity in fullerides," Rev. Mod. Phys. **69**, 575 (1997).

[22] O. Gunnarsson, *Alkali-Doped Fullerides: Narrow-Band Solids with Unusual Properties* (World Scientific, Singapore, 2004).

[23] A. Auerbach, N. Manini, and E. Tosatti, "Electron-vibron interactions in charged fullerenes. I. Berry phases," Phys. Rev. B **49**, 12998 (1994).

[24] N. Manini, E. Tosatti, and A. Auerbach, "Electron-vibron interactions in charged fullerenes. II. Pair energies and spectra," Phys. Rev. B **49**, 13008 (1994).

[25] M. C. M. O'Brien, "Vibronic energies in $C_{60}{}^{n-}$ and the Jahn-Teller effect," Phys. Rev. B **53**, 3775 (1996).

[26] L. F. Chibotaru, "Spin-Vibronic Superexchange in Mott-Hubbard Fullerides," Phys. Rev. Lett. **94**, 186405 (2005).

[27] Y. Nomura, S. Sakai, M. Capone, and R. Arita, "Exotic s-wave superconductivity in alkali-doped fullerides,"

J. Phys.: Condens. Matter **28**, 153001 (2016).

[28] A. Nava, C. Giannetti, A. Georges, E. Tosatti, and M. Fabrizio, "Cooling quasiparticles in A_3C_{60} fullerides by excitonic mid-infrared absorption," Nat. Phys. **14**, 154 (2018).

[29] N. Iwahara, "Berry phase of adiabatic electronic configurations in fullerene anions," Phys. Rev. B **97**, 075413 (2018).

[30] N. Iwahara, T. Sato, K. Tanaka, and L. F. Chibotaru, "Vibronic coupling in C_{60}^- anion revisited: Derivations from photoelectron spectra and DFT calculations," Phys. Rev. B **82**, 245409 (2010).

[31] N. Iwahara and L. F. Chibotaru, "Dynamical Jahn-Teller Effect and Antiferromagnetism in Cs_3C_{60}," Phys. Rev. Lett. **111**, 056401 (2013).

[32] D. Liu, N. Iwahara, and L. F. Chibotaru, "Dynamical Jahn-Teller effect of fullerene anions," Phys. Rev. B **97**, 115412 (2018).

[33] N. Iwahara and L. F. Chibotaru, "Dynamical Jahn-Teller instability in metallic fullerides," Phys. Rev. B **91**, 035109 (2015).

[34] N. Iwahara and L. F. Chibotaru, "Orbital disproportionation of electronic density is a universal feature of alkali-doped fullerides," Nat. Commun. **7**, 13093 (2016).

[35] In the inequivalent subbands, the electron correlation develops in different ways. The evolution of the electron correlation can be seen in the Gutzwiller's reduction factors with respect to Coulomb repulsion on C_{60} sites (see Fig. 2d in Ref. [34]). As the increase of the Coulomb repulsion on C_{60} sites the Gutzwiller's factor of half-filled subband becomes close to zero (strongly correlated), whereas those for empty and filled subbands become close to one (uncorrelated). Since the metallic screening and the band energy for nondegenerate system are smaller than those of degenerate band, the critical Coulomb repulsion on C_{60} sites for the Mott transition is smaller too (Sec. VI in Ref. [33]).

[36] Y. Matsuda, S. Heguri, and K. Tanigaki, in preparation.

[37] V. Brouet, H. Alloul, S. Garaj, and L. Forró, "Persistence of molecular excitations in metallic fullerides and their role in a possible metal to insulator transition at high temperatures," Phys. Rev. B **66**, 155124 (2002).

[38] P. Jeglič, D. Arčon, A. Potočnik, A. Y. Ganin, Y. Takabayashi, M. J. Rosseinsky, and K. Prassides, "Low-moment antiferromagnetic ordering in triply charged cubic fullerides close to the metal-insulator transition," Phys. Rev. B **80**, 195424 (2009).

[39] The calculations in Ref. [33] show unquenched dynamical JT effect on the C_{60}^{3-} sites in Cs_3C_{60} which is gradually quenched approaching the limit of JT glass in fullerides of a smaller volume like K_3C_{60}. The observed transformation of the shape of the IR line can be related to this change of the character of JT effect but not to its full disappearance as was supposed in Ref. [18]. See also Sec. VI.

[40] H. Alloul, P. Wzietek, T. Mito, D. Pontiroli, M. Aramini, M. Riccò, J. P. Itie, and E. Elkaim, "Mott Transition in the $A15$ Phase of Cs_3C_{60}: Absence of a Pseudogap and Charge Order," Phys. Rev. Lett. **118**, 237601 (2017).

[41] See Supplemental Materials at [URL] for the definition of normal modes, symmetrized quadratic polynomials of coordinates, DFT data, assignment of the vibronic states and transition dipole intensities.

[42] Y. Nomura, K. Nakamura, and R. Arita, "Ab initio derivation of electronic low-energy models for c_{60} and aromatic compounds," Phys. Rev. B **85**, 155452 (2012).

[43] Displacement $u_{A\lambda}$ of nuclei A along λ $(= x, y, z)$ direction from a high-symmetric reference structure is expressed by mass-weighted coordinates as $u_{A\lambda} = \sum_{\mu\Gamma\gamma} q_{\Gamma(\mu)\gamma} e_{A\lambda}^{\Gamma(\mu)\gamma}/\sqrt{M_A}$, where M_A is the mass of nucleus A, and $e_{A\lambda}^{\Gamma(\mu)\gamma}$ is the polarization vector of $\Gamma(\mu)\gamma$ normal mode. The polarization vector is dimensionless, and the dimension of $q_{\Gamma\gamma}$ is $\sqrt{m_e}a_0$, where m_e is mass of electron and a_0 is Bohr radius. See for detail Sec. 10.1 in Ref. [61].

[44] G. Racah, "Theory of Complex Spectra. III," Phys. Rev. **63**, 367 (1943).

[45] D. Liu, Y. Niwa, N. Iwahara, T. Sato, and L. F. Chibotaru, "Quadratic Jahn-Teller effect of fullerene anions," Phys. Rev. B **98**, 035402 (2018).

[46] The orders of the obtained quadratic coupling parameters V and the expectation value of the product of IR coordinates $\hat{q}^2$ are 10^{-7} a.u. and 10^2 a.u., respectively, therefore, the energy scale of each quadratic vibronic coupling $\sqrt{15/2}V\langle\hat{q}^2\rangle$ is 10^{-5}-10^{-4} a.u. Here, $\langle\hat{q}^2\rangle$ is approximated as $(\hbar/\omega)(\langle\hat{n}\rangle + 1/2)$ using the harmonic oscillator model with $\omega \approx 1350$ cm^{-1} and the averaged vibrational quantum number $\langle\hat{n}\rangle$ = 0-1. On the other hand, the energy scale of the linear vibronic coupling is 10^{-3} a.u. in terms of the JT energy for C_{60}^-.

[47] Both the IR active $t_{1u}(4)$ and inactive $g_u(5)$ and $h_u(6)$ modes are called IR modes because these three modes are admixed by the quadratic vibronic coupling, resulting in the contribution to the fine structure of the IR spectrum.

[48] In this work, we treat two types of vibronic states. The first ones are the eigenstates of linear $t_{1u}^3\otimes 8h_g$ JT Hamiltonian and the second are eigenstates of the full Hamiltonian $\hat{H}$, including nonlinear vibronic couplings to the IR modes. To avoid the confusion, we call the former JT states and the latter vibronic states.

[49] J. J. Sakurai, *Modern quantum mechanics (revised edition)* (Addison-Wesley, Boston, 1994).

[50] At higher temperature above 150 K, many peaks from these excited JT levels above the T_{1u} and H_u ones and the broadening of the line width smear the shape of the fine structures of the IR spectrum.

[51] The slight difference between the theoretical and experimental shapes of the main peaks might be explained by the small shift of the theoretical vibronic levels from the real ones due to e.g. the absence of weak intersite interactions and crystal field effect in our calculations or the imperfect agreement between the DFT and experimental parameters. One also should note the sample dependence of IR spectra: Although both experimental data show the growth of new peak as the rise of temperature, the main peaks at 28 K at the bottom and the top of Fig. 2 (d) have slightly different fine structures.

[52] W. R. Thorson, "Vibronically Induced Absorption of Forbidden Infrared Transitions," J. Chem. Phys. **29**, 938 (1958).

[53] S. S. Naghavi, M. Fabrizio, T. Qin, and E. Tosatti, "Nanoscale orbital excitations and the infrared spectrum of a molecular Mott insulator: $A15$-Cs_3C_{60}," Nanoscale **8**, 17483 (2016).

[54] M. Mitrano, A. Cantaluppi, D. Nicoletti, S. Kaiser, A. Perucchi, S. Lupi, P. Di Pietro, D. Pontiroli, M. Riccó, S. R. Clark, D. Jaksch, and A. Cavalleri, "Possible light-

induced superconductivity in K_3C_{60} at high temperature," Nature **530**, 461 (2016).

[55] A. Cantaluppi, M. Buzzi, G. Jotzu, D. Nicoletti, M. Mitrano, D. Pontiroli, M. Riccó, A. Perucchi, P. Di Pietro, and A. Cavalleri, "Pressure tuning of light-induced superconductivity in K_3C_{60}," Nat. Phys. **14**, 837 (2018).

[56] D. M. Kennes, E. Y. Wilner, D. R. Reichman, and A. J. Millis, "Transient superconductivity from electronic squeezing of optically pumped phonons," Nat. Phys. **13**, 479 (2017).

[57] M. A. Sentef, "Light-enhanced electron-phonon coupling from nonlinear electron-phonon coupling," Phys. Rev. B **95**, 205111 (2017).

[58] D. A. Varshalovich, A. N. Moskalev, and V. K. Khersonskii, *Quantum Theory of Angular Momentum* (World Scientific, Singapore, 1988).

[59] M. J. Frisch, G. W. Trucks, H. B. Schlegel, G. E. Scuseria, M. A. Robb, J. R. Cheeseman, G. Scalmani, V. Barone, B. Mennucci, G. A. Petersson, H. Nakatsuji, M. Caricato, X. Li, H. P. Hratchian, A. F. Izmaylov, J. Bloino, G. Zheng, J. L. Sonnenberg, M. Hada, M. Ehara, K. Toyota, R. Fukuda, J. Hasegawa, M. Ishida, T. Nakajima, Y. Honda, O. Kitao, H. Nakai, T. Vreven, J. A. Montgomery, Jr., J. E. Peralta, F. Ogliaro, M. Bearpark, J. J. Heyd, E. Brothers, K. N. Kudin, V. N. Staroverov, R. Kobayashi, J. Normand, K. Raghavachari, A. Rendell, J. C. Burant, S. S. Iyengar, J. Tomasi, M. Cossi, N. Rega, J. M. Millam, M. Klene, J. E. Knox, J. B. Cross, V. Bakken, C. Adamo, J. Jaramillo, R. Gomperts, R. E. Stratmann, O. Yazyev, A. J. Austin, R. Cammi, C. Pomelli, J. W. Ochterski, R. L. Martin, K. Morokuma, V. G. Zakrzewski, G. A. Voth, P. Salvador, J. J. Dannenberg, S. Dapprich, A. D. Daniels, . Farkas, J. B. Foresman, J. V. Ortiz, J. Cioslowski, and D. J. Fox, "Gaussian09 Revision D.01," Gaussian Inc. Wallingford CT 2009.

[60] The program for the calculation of $|\Psi_\tau\rangle$ and IR spectra is available at https://github.com/quasi-human.

[61] T. Inui, Y. Tanabe, and Y. Onodera, *Group Theory and Its Applications in Physics* (Springer-Verlag, Berlin and Heidelberg, 1990).